Chapter 5
Influence of Measurement Parameters on Giant Magnetoimpedance

In this chapter, the influences of the measurement parameters (e.g. alternating current, dc magnetic field, frequency, and temperature) on giant magnetoimpedance (GMI) have been systematically analysed and clarified. This ensures the selection of optimal conditions for designing high-performance GMI-based sensors.

5.1 Alternating Current Amplitude

When a magnetic wire is subjected to a GMI experiment (Fig. 4.4), a circular magnetisation process takes place in it due to the ac circular magnetic field created by an alternating current (I_{ac}). Any change in I_{ac} will result in a change in the circular permeability (μ_ϕ) and hence the ac impedance, Z. This points to a dependence of the impedance on the current; the higher the current amplitude, the larger the expected value of the impedance. It has been theoretically predicted that for a double-peak (DP) profile of GMI in ferromagnetic amorphous wires, the magnetic field (H_K) at which the value of Z reaches a maximum should decrease as the amplitude of the ac current is increased [1]. This hypothesis has been experimentally confirmed (see Fig. 5.1, for example, for a Co-based amorphous wire), where GMI curves are found to exhibit a DP behaviour for low-amplitude currents where only reversible wall motion takes place, but only a single peak (SP) is observed at high amplitudes corresponding to circular coercivity [2].

Through investigating the dependence of GMI on ac in different materials (e.g. amorphous microwires/wires, nanocrystalline ribbons), Aragoneses et al. [3] found the variation of the GMI effect with current amplitude to be material-dependent. For an amorphous $Co_{68.5}Mn_{6.5}Si_{10}B_{15}$ microwire, when I_{ac} was increased the GMI effect increased until $I_{ac} = 2.8$ mA and then decreased at higher values of I_{ac}. This is consistent with the behaviour of an $(Fe_6Co_{94})_{72.5}Si_{12.5}B_{15}$ amorphous wire, where the maximum GMI effect was achieved for $I_{ac} = 4$ mA, as I_{ac} was varied from 2 to 7 mA [4]. With increasing I_{ac}, however, the GMI effect decreased gradually for an

H.-X. Peng et al., *Ferromagnetic Microwire Composites*,
Engineering Materials and Processes, DOI 10.1007/978-3-319-29276-2_5

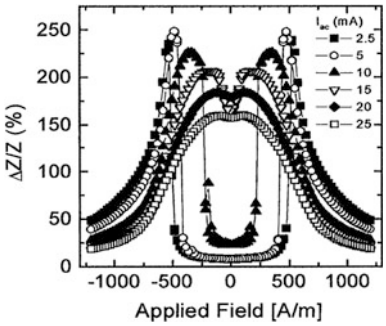

Fig. 5.1 Magnetic field dependence of the GMI ratio ($\Delta Z/Z$) at different alternating current amplitudes (I_{ac}) for a Co-based amorphous wire with an induced circular anisotropy. An evolution from the DP to SP feature with increasing amplitude has been observed (reproduced with permission from Elsevier [2])

$(Fe_{0.94}Co_{0.06})_{72.5}B_{15}Si_{12.5}$ amorphous wire, while it sharply increased for a $Fe_{73.5}Si_{13.5}B_9Nb_3Cu_1$ nanocrystalline ribbon [3]. In these examples, the observed effect of driving current could be explained by consideration of the tensor character of the magnetic permeability and was ascribed to the components of that tensor which are responsible for the transverse magnetic anisotropy [5]. The different dependences of GMI on driving alternating current can also be caused by the difference in the domain structures of the investigated samples. It is worth noting that there is an inhomogeneous distribution of local critical magnetic fields at low-amplitude currents, causing the "spike" feature in GMI profiles or the instability of the GMI signal. Increasing the amplitude has been shown to greatly improve the stability of the GMI signal [6]. It is therefore important to select an appropriate range of current amplitudes for the design and operation of actual GMI sensor devices.

5.2 Magnetic Field

In a typical GMI experiment, the dc magnetic field is usually applied so as to be collinear with the alternating current along the longitudinal direction of the wire (Fig. 4.4). This configuration yields the longitudinal GMI effect. As discussed previously in Chap. 4, at a given frequency, the application of a dc magnetic field (H_{dc}) changes the circular permeability (μ_ϕ) and hence the magnetic penetration depth (δ_m), which in turn alters the impedance Z until the value of δ_m reaches the radius of the wire (t). In a magnetic amorphous wire with a circular domain structure, H_{dc} may compensate the circular magnetic anisotropy field (H_k) as its magnitude becomes similar [2, 7]. For $H_{dc} \cong H_k$, the quasi-free magnetisation responds quickly to the external oscillating magnetic field, giving rise to the maximum circular permeability. When the applied dc magnetic field exceeds the

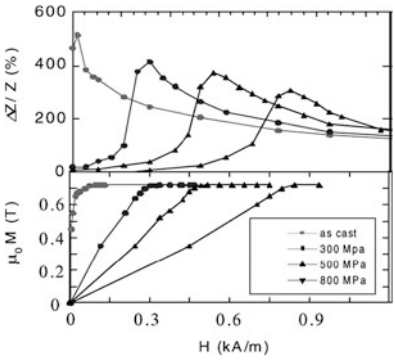

Fig. 5.2 Magnetic field dependence of the GMI ratio and axial magnetisation curves for a stress-annealed Co-based wire (different tensile stresses were applied during annealing). This shows a correlation between the maximum GMI values and circular anisotropy fields (reproduced with permission from Elsevier [2])

circular magnetic anisotropy field ($H_{dc} > H_k$), the circular permeability is decreased due to the unidirectional magnetostatic anisotropy caused by H_{dc}. In this case, the skin depth increases, which corresponds to the decrease of the impedance of the wire as the dc magnetic field is increased. Since the value of the anisotropy field is actually very small in magnetic wires in which the magnetostriction constant is near zero, the maximum value of GMI is observed at nearly zero field for low frequencies [8]. As a result, the GMI profile shows an SP behaviour centred around zero field. At higher frequencies, however, GMI profiles will show a DP feature. Such SP and DP features of GMI are often determined by the relative contribution from domain wall motion and magnetisation rotation processes to the circular permeability [9–11]. Complex domain structures and distribution of local anisotropies in actual materials can also influence the dependence of GMI on the dc magnetic field [12].

When studying the effects of tensile stress on the dc magnetisation and GMI of a Co-based wire, Vazquez has demonstrated the existence of a correlation between the circular magnetic anisotropy field and the GMI peak [2]. As can be clearly seen in Fig. 5.2, the GMI magnitude and the circular anisotropy field decrease as the applied stress is increased. The magnetic field at which the GMI peak is observed consistently corresponds to the circular magnetic anisotropy field determined from the magnetisation data and this field increases with an increase in the applied stress.

5.3 Measurement Frequency

According to the theory (Chap. 4), GMI and its behaviour depend strongly on the measurement frequency. Indeed, the frequency-dependent GMI features have been experimentally studied in a wide range of frequencies up to GHz in different

materials [12]. It has been shown that, with increasing frequency, the magnetisation process via domain wall displacement relaxes at relatively low frequencies ranging between 0.1 and 1 MHz in amorphous wires [13]. For amorphous glass-covered microwires, the permeability spectra showed dispersion laws at higher frequencies [14]. It is generally accepted that at low frequencies $f \ll f_o$—a characteristic frequency or the frequency at which the maximum GMI value is obtained ($a < \delta_m$), the maximum value of GMI, $[\Delta Z/Z(\%)]_{\max}$, is found to be relatively low due to the contribution of the induced magnetoinductive voltage to magnetoimpedance [15]. In this case, GMI features can be well interpreted on the basis of the quasi-static models, as discussed in Chap. 4. As $f \sim f_o$ ($a \approx \delta_m$), the skin effect is dominant, and a higher $[\Delta Z/Z(\%)]_{\max}$ is found. Beyond $f \geq f_o$, $[\Delta Z/Z(\%)]_{\max}$ decreases with increasing frequency. It is believed that, in this frequency region, the domain wall displacement is strongly damped by eddy currents, thus contributing less to the circular permeability, i.e. a small $[\Delta Z/Z(\%)]_{\max}$. A typical example of this dependence is shown in Fig. 4.6b. We should note here that the magnetoimpedance is increasing as the frequency increases because the impedance is proportional to $(\omega\mu_\phi)^{1/2}$ even in the case of decreasing circular permeability at high frequencies. Despite this, f_o depends strongly on the dimensions of the samples. It has been found that, for amorphous microwires, GMI usually reaches its maximum value at higher frequencies than those for amorphous wires [16]. The eddy current and domain models are valid for interpreting basic GMI features in the frequency range of 0.1–100 MHz, as discussed in Chap. 4. At higher frequencies, where ferromagnetic resonance can occur, such GMI features were successfully explained by the electromagnetic and exchange-conductivity models [17]. Furthermore, with increasing frequency, the low-frequency SP behaviour may become DP-like as a consequence of the frequency dependence of circular permeability [2].

From a fundamental research viewpoint, it is essential to understand the frequency dependences of the real and imaginary parts of impedance and their contributions to the GMI effect. Figure 5.3 shows, for example, the frequency dependences of the maximum MR, MX, and MI ratios for a glass-coated amorphous microwire. It is generally thought that the MX contribution to the MI ratio is dominant at the low-frequency range, while the main contribution to the MI in the high-frequency range can be attributed to the MR. As one can see in Fig. 5.3, however, the frequency dependence of MI follows that of MR, suggesting the dominant contribution of MR to the MI for the case of this microwire throughout the investigated frequency range.

From an experimental point of view, we should note that most GMI measurements are performed at measuring frequencies up to 10 MHz only, due to the fact that, in this frequency range, standard voltage–current measurement techniques can be easily employed to directly probe the transport properties of the sample. At higher frequencies, both voltage and current are not always well defined quantitatively and the classic measurement technique fails. To overcome this problem, another technique based on the S-parameter measurement of a transmission line section by means of an automatic vectorial network analyser has been exploited to measure the GMI effect in the microwave region in soft amorphous ferromagnetic samples [18].

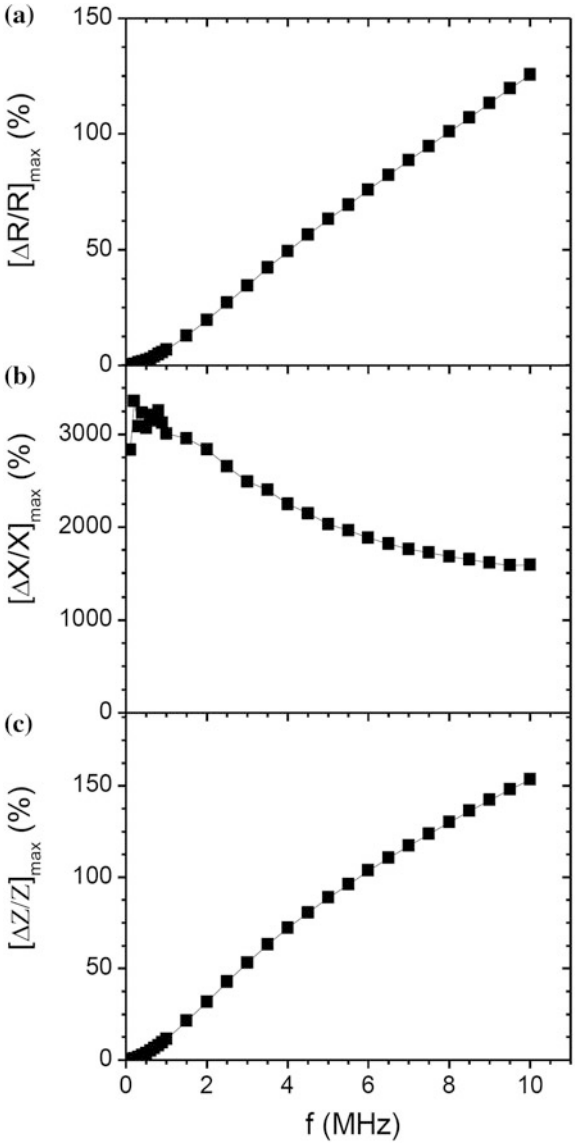

Fig. 5.3 Frequency dependence of the maximum magnetoresistance (*MR*), magnetoreactance (*MX*), and magnetoimpedance (*MI*) ratios of soft ferromagnetic amorphous glass-coated $Co_{68}B_{15}Si_{10}Mn_7$ microwire

5.4 Measurement Temperature

A thorough knowledge of the measurement temperature dependence of GMI is important and necessary from both the fundamental and practical points of view. A number of works have investigated the influence of the measurement temperature on GMI in magnetic amorphous wires [19–23]. It is now accepted that the GMI

effect increases with temperature and reaches a maximum value near the Curie temperature of the material, and then decreases at higher temperatures [19, 21, 23]. The initial increase of GMI with temperature is attributed to the rise in circular permeability resulting from the enhanced circular motion of magnetic moments which are frozen at low temperature. It is believed that the magnetic coupling between magnetic moments at a low temperature is larger than that at a high temperature. The maximum of GMI is achieved close to the Curie temperature because the largest value of circular permeability is achieved at this temperature. It has been reported that the magnitude of GMI of an amorphous $Co_{68.15}Fe_{4.35}Si_{12.5}B_{15}$ wire measured at 300 K ($\sim T_C$) was about two times larger than that measured at 100 K [19]. At temperatures above the Curie point, the observed decrease of GMI is ascribed to the collapse of the magnetic coupling in the material [21].

Figure 5.4 shows the results of a study of the effects of three consecutive sweeps in temperature from 80 to 400 K for an amorphous $Co_{68.15}Fe_{4.35}Si_{12.5}B_{15}$ wire with a diameter of 130 μm, which was prepared using the in-rotating water quenching technique [19]. It is worth noting that there is a significant reduction in the GMI magnitude as well as a displacement of the GMI maximum in temperature. It has been suggested that in the first sweep a slight increase of the temperature determines a reversible relaxation of internal stresses induced during rapid solidification, which results in a slight reduction of the circular anisotropy and hence an improvement of the magnetic softness of the wire without alternating its specific circular magnetic structure [19]. Once the first temperature sweep is completed, stress annealing and atomic diffusion are believed to manifest in the wire when passing the Curie temperature. These processes last until thermal equilibrium is re-established in the wire at room temperature. This sets in a new temperature for the GMI maximum and a new temperature maximum of the circular permeability, which are observed in the subsequent temperature sweep. Magnetic hysteresis measurements were conducted around the Curie temperature after each sweep to determine whether the effects of temperature processes on the static magnetic properties are significant. As one can see in Fig. 5.4b, changes in the M–H loops are not very large, unlike the

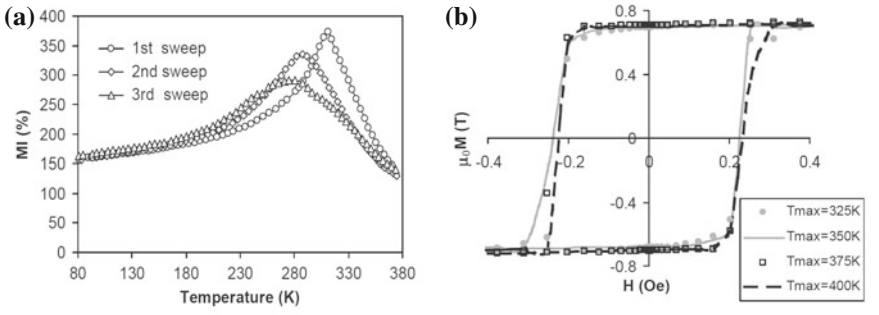

Fig. 5.4 **a** Temperature dependence of the MI ratio of an amorphous $Co_{68.15}Fe_{4.35}Si_{12.5}B_{15}$ wire for three consecutive temperature sweeps. **b** Hysteresis loops after temperature processing (reproduced with permission from Elsevier [19])

GMI data obtained at the corresponding temperatures. However, we should note that the data obtained from a VSM reflect the bulk magnetic property of the wire, while the GMI profile provides near-surface magnetic information.

5.5 Concluding Remarks

Because the measurement parameters (alternating current, dc magnetic field, and frequency) directly affect the measured value of GMI, the selection of appropriate parameters becomes extremely important in designing practical GMI sensors. Depending upon the different kinds of GMI materials, the amplitude of an applied alternating current should be large or small. Similarly, the maximum dc magnetic field applied to saturate the magnetoimpedance varies among GMI materials. However, for practical uses, the amplitude of the applied current and the maximum dc magnetic field should be as small as possible. Furthermore, because of the magnitude of GMI and the way in which its sensitivity varies strongly with measurement frequency, it is necessary to select the working frequency range for a certain material. At relatively low frequencies such as these, it should be noted that the SP behaviour of GMI is often observed and this is usually useful for practical applications. In contrast, the DP behaviour of GMI observed in the high-frequency range is not desirable. However, such a symmetrical feature in low-field GMI profiles can be tailored for developing a new class of linear field sensors. Finally, it is worth noting that a sensor based on the GMI effect has an increasing sensitivity at room temperature because the Curie temperatures of GMI materials are well above 300 K, whereas the field sensitivity of a magnetic sensor based on the giant magnetoresistance (GMR) effect in thin films and in perovskite-like structured materials is drastically reduced at room temperature. Therefore, for practical use, GMI-based sensors are more promising than the GMR sensors.

References

1. Chen DX, Munoz JL, Hernando A, Vazquez M (1998) Magnetoimpedance of metallic ferromagnetic wires. Phys Rev B 57:10699–10704
2. Vazquez M (2001) Giant magnetoimpedance in soft magnetic “wires”. J Magn Magn Mater 226–230:693–699
3. Aragoneses P, Zhukov A, Gonzalez J, Blanco JM, Dominguez L (2000) Effect of AC driving current on magneto-impedance effect. Sen Act A 81:86–90
4. Pal SK, Manik NB, Mitra A (2006) Dependence of frequency and amplitude of the ac current on the GMI properties of Co based amorphous wires. Mater Sci Eng A 415:195–201
5. Chen AP, Britel MR, Zhukova V, Zhukov A, Dominguez L, Chizhik AB, Blanco JM, González J (2004) Influence of AC magnetic field amplitude on the surface magnetoimpedance tensor in amorphous wire with helical magnetic anisotropy. IEEE Trans Magn 40:3368–3377

6. Sun J-F, Liu J-S, Xing D-W, Xue X (2011) Experimental study on the effect of alternating-current amplitude on GMI output stability of Co-based amorphous wires. Phys Status Solidi A 208(4):910–914
7. Mandal K, Pan Mandal S, Vazquez M, Puerta S, Hernando A (2002) Giant magnetoimpedance effect in a positive magnetostrictive glass-coated amorphous microwire. Phys Rev B 65:064402, 1–6
8. Devkota J, Ruiz A, Mukherjee P, Srikanth H, Phan MH (2013) Magneto-resistance, magneto-reactance, magneto-impedance effects in single and multi-wire systems. J Alloy Compd 549:295
9. Usov NA, Gudoshnikov SA (2013) Giant magneto-impedance effect in amorphous ferromagnetic wire with a weak helical anisotropy: theory and experiment. J Appl Phys 113:243902
10. Lachowicz HK, Garcia KL, Kuzminski M, Zhukov A, Vazquez M (2005) Skin-effect and circumferential permeability in micro-wires utilized in GMI-sensors. Sens Act A 119:384–389
11. Pirota KR, Kraus L, Chiriac H, Knobel M (2000) Magnetic properties and giant magnetoimpedance in a CoFeSiB glass-covered microwire. J Magn Magn Mater 221: L243–L247
12. Phan MH, Peng HX (2008) Giant magnetoimpedance materials: fundamentals and applications. Prog Mater Sci 53:323–420
13. Kim CG, Yoon SS, Yu SC (2000) Decomposition of susceptibility spectra in a torsion-stressed Fe-based amorphous wire. Appl Phys Lett 76:3463–3465
14. Zhukov A, González J, Vázquez M, Larin V, Torcunov A (2004) Nanocrystalline and amorphous magnetic microwires. In: Nalwa HS (ed) Encyclopedia of nanoscience and nanotechnology, vol 23, Chap. 62. American Scientific Publishers, pp 1–22
15. Mohri K, Kohsawa T, Kawashima K, Yoshida H, Panina LV (1992) Magneto-inductive effect (MI effect) in amorphous wires. IEEE Trans Magn 28:3150–3152
16. Chiriac H, Ovari TA (1996) Amorphous glass-covered magnetic wires: preparation, properties, applications. Prog Mater Sci 40:333–407
17. Ciureanu P, Melo LGC, Seddaoui D, Ménard D, Yelon A (2007) Physical models of magnetoimpedance. J Appl Phys 102:073908
18. Zhukov A, Zhukova V, Blanco JM, Gonzalez J (2005) Recent research on magnetic properties of glass-coated microwires. J Magn Magn Mater 294(2):182–192
19. Chiriac H, Marinescu CS, Ovari TA (1999) Temperature dependence of the magneto-impedance effect. J Magn Magn Mater 196–197:162–163
20. Rakhmanov AA, Perov N, Sheverdyaeva P, Granovsky A, Antonov AS (2003) The temperature dependence of the magneto-impedance effect in the Co-based amorphous wires. Sens Actuators A 106:240–242
21. Hernando B, Olivera J, Sánchez ML, Prida VM, Varga R (2008) Temperature dependence of magnetoimpedance and anisotropy in nanocrystalline finemet wire. IEEE Trans Magn 44:3965
22. Wang XD, Liu JS, Xing DW, Chen DM, Wang H, Sun JF (2013) Thermal stability of giant magneto-impedance effect in glass-covered amorphous wires. Phys Procedia 48:152–159
23. Liu J-S, Sun J-F, Xing D-W, Xue X (2012) Twin-detector sensor of Co-rich amorphous microwires to overcome GMI fluctuation induced by ambient temperature. IEEE Trans Magn 48:2449